

ornl

**OAK RIDGE
NATIONAL
LABORATORY**

LOCKHEED MARTIN 

MANAGED AND OPERATED BY
LOCKHEED MARTIN ENERGY RESEARCH CORPORATION
FOR THE UNITED STATES
DEPARTMENT OF ENERGY

ORNL-27 (3-96)

RECEIVED
FEB 12 1997
OSTI

ORNL/TM-13159

EVALUATION OF DEMO 1C COMPOSITE FLYWHEEL ROTOR BURST TEST AND CONTAINMENT DESIGN

M. D. Kass
J. W. McKeever
M. A. Akerman
P. L. Goranson
P. S. Litherland
D. U. O'Kain

Oak Ridge National Laboratory

Approved for public release;
distribution is unlimited.

MASTER

Prepared by
Oak Ridge National Laboratory
Oak Ridge, Tennessee 37831-8088
managed by
LOCKHEED MARTIN ENERGY RESEARCH CORP.
for the
U.S. DEPARTMENT OF ENERGY
under contract DE-AC05-96OR22464 

DISTRIBUTION OF THIS DOCUMENT IS UNLIMITED

This report has been reproduced directly from the best available copy.

Available to DOE and DOE contractors from the Office of Scientific and Technical Information, P.O. Box 62, Oak Ridge, Tennessee 37831; prices available from (423) 576-8401.

Available to the public from the National Technical Information Service, U.S. Department of Commerce, 5285 Port Royal Road, Springfield, Virginia 22161.

This report was prepared as an account of work sponsored by an agency of the United States Government. Neither the United States Government nor any agency thereof, nor any of their employees, makes any warranty, express or implied, or assumes any legal liability or responsibility for the accuracy, completeness, or usefulness of any information, apparatus, product, or process disclosed, or represents that its use would not infringe privately owned rights. Reference herein to any specific commercial product, process, or service by trade name, trademark, manufacturer, or otherwise, does not necessarily constitute or imply its endorsement, recommendation, or favoring by the United States Government or any agency thereof. The views and opinions of authors expressed herein do not necessarily state or reflect those of the United States.

DISCLAIMER

Portions of this document may be illegible electronic image products. Images are produced from the best available original document.

**EVALUATION OF DEMO 1C COMPOSITE FLYWHEEL ROTOR BURST
TEST AND CONTAINMENT DESIGN**

M. D. Kass
J. W. McKeever
M. A. Akerman
P. L. Goranson
P. S. Litherland
D. U. O'Kain

Prepared by the
Oak Ridge National Laboratory
Oak Ridge, Tennessee 37831
managed by
LOCKHEED MARTIN ENERGY RESEARCH CORP.
for the
U.S. DEPARTMENT OF ENERGY
under Contract No. DE-AC05-96OR22464

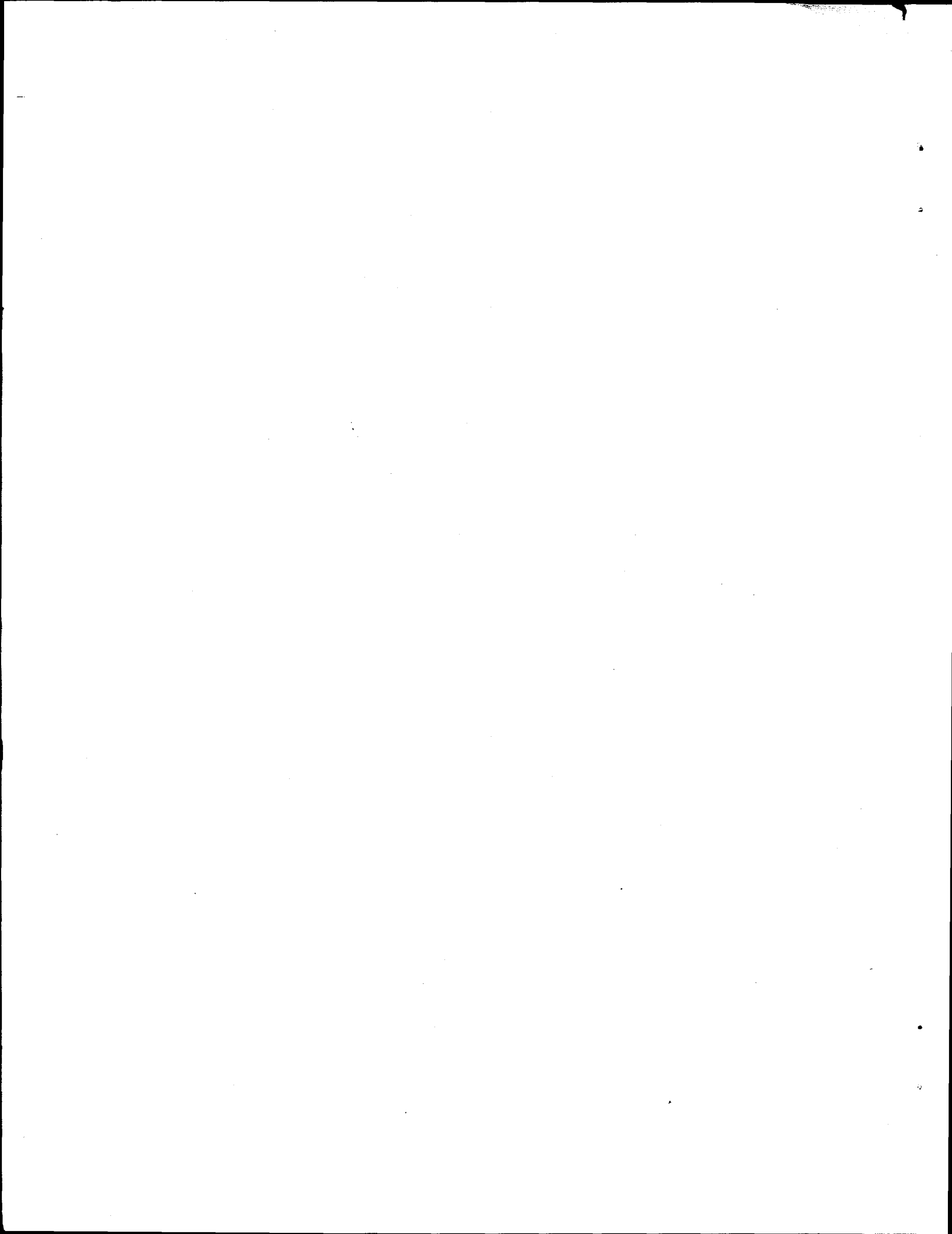


TABLE OF CONTENTS

EXECUTIVE SUMMARY	v
1. SUMMARY	1
2. BACKGROUND	1
3. INTRODUCTION	1
4. FLYWHEEL ENERGY	2
5. FAILURE MECHANISMS	4
6. LIGHTWEIGHT MATERIAL AND LAYERING CONTAINMENT CONCEPTS	8
7. FABRICATION AND ASSEMBLY	8
8. CONCLUSIONS	10
9. RECOMMENDATIONS	10
10. REFERENCES	11
11. APPENDIX A	13

EXECUTIVE SUMMARY

Flywheel energy storage is being considered for use in a variety of electric utility applications and for use in electric vehicles and hybrid electric vehicles. Flywheels offer excellent high power performance characteristics, and their use as a peak power unit in hybrid electric vehicles takes advantage of these characteristics. A number of flywheel programs are being funded by the Department of Energy (DOE), the Advanced Research Projects Agency (ARPA), the U.S. big three automakers, and by private investment.

A key technical issue associated with the implementation of flywheel technology is the development of effective, light-weight, low-cost containment systems. Development of effective containment systems is a process that requires extensive experimental testing to verify the analytical predictions. This lab directed project provides an evaluation and analysis of the fundamental loads produced in the failure of a high-speed composite flywheel rotor and considers some of the design features of the required containment system. It is recognized that the probability of a rotor burst failure depends highly on the design of the rotor and also the design of the overall system, including bearings, motor/generator, and other design features. The probability of failure will depend also on the operating environment (shock loads, temperatures, etc.). It is also recognized that the nature of the failure and the resulting loads is highly dependent on rotor design (control of critical stress regions) and operating parameters (stress margins). This project seeks to establish fundamental understanding of basic principles which can be used in the design and evaluation of any new flywheel configuration.

A key result of this project was an improved understanding and documentation of the results of the Oak Ridge National Laboratory (ORNL) Demo 1C flywheel test, which was performed in 1985. Detailed investigation and evaluation of the damage to the spin tank with corresponding analytical explanations are provided in this report. An analysis of the physics of failure of a flywheel rim is provided. A simple method of estimating the required containment is also suggested. Finally, some of the basic limitations on the geometry of the flywheel containment are evaluated with respect to assembly methods, and a conceptual layout of a composite reinforced containment housing is provided. As the result of the analysis, several key conclusions are reached. The basic information provided should be useful in supporting the design and fabrication of actual containment housings and in understanding the experimental test results. This project was initiated in April 1995 with a completion date of October 31, 1995.

In August 1995, an accident involving a flywheel containment test occurred in Europe and resulted in the death of one of the operators. The accident heightened awareness of the seriousness of safety and containment for flywheels. DOE is initiating a new program in FY 1996 to investigate flywheel safety and containment, with work to be done at ORNL and Lawrence Livermore National Laboratory (LLNL). The program will be coordinated with flywheel development work being done at ARPA contractors.

1. SUMMARY

Laboratory-Directed funds were provided in FY 1995 for research to develop flywheel containment specifications and to consider concepts that could satisfy these specifications and produce a prototype small, lightweight, inexpensive, mobile flywheel containment. Research activities have included an analytical and pictorial review of the Demo 1C flywheel failure test, which provided significant insight about radial and axial failure modes; calculations of the thickness of ultra-conservative pressure vessel containment; entertainment of advanced containment concepts using lightweight materials and armor literature; consideration of fabrication assembly procedures; and participation in a Flywheel Energy Storage Workshop during which additional flywheel failure experiences were discussed. Based on these activities, calculations, and results, a list of conclusions concerning flywheel containment and its relation to the flywheel are presented followed by recommendations for further research.

2. BACKGROUND

The importance of flywheel energy storage (FES) is increasing with the discovery of better materials and new technologies. FES may be used for a range of energy storage applications from leveling a utility company's electric power to extending the range of an automobile. By far, the most challenging is the mobile automobile application.

Three technologies are considered enabling for the mobile FES. They are (1) electronic systems capable of transferring power back and forth between the flywheel and the electric motor, (2) magnetic or mechanical bearing systems that can operate at the rotational speeds desired and that have acceptable lifetimes, and (3) safety and containment. This paper is concerned with mobile flywheel containment systems. To be useful in the Partnership for a New Generation of Vehicles (PNGV) the containment must be small, light, inexpensive, and safe. The chance for success is increased if advanced composite materials are used, but that tends to increase the cost. Tradeoff studies are essential, but will only be effective if specifications without excessive safety factors may be determined.

Much of the past flywheel research has involved understanding and controlling the energy released during failure of rotating components (1-10). Past testing has indicated the necessity of a rugged containment system. Rotatable inner liners have been used to absorb the kinetic energy.

3. INTRODUCTION

The objective of the project is to propose innovative mobile automotive flywheel containment concepts in light of ORNL's broad spin test experience accumulated during 30 years in DOE's Uranium Enrichment Programs. A significant test was performed at ORNL on December 9, 1985, when the Demo 1C flywheel was spun to failure at a rim energy of 1.51 kWh. This failure occurred at a peripheral velocity of 1405 m/s near the ultimate strength of the rim, which comprised two concentric circumferentially wound carbon fiber reinforced epoxy rings with radial thickness of 0.75-in. and axial height of 1.87-in. The outer ring, whose reinforcement was IM6, had a 27-in. O.D. and the inner ring, whose reinforcement was AS6, had a 24-in. I.D. The rim was fabricated by six sequential wind-and-cure operations, with each operation adding approximately 0.25-in. radial thickness. The flywheel system, located in ORNL's revetment spin test facility, was doubly contained by a 2-in. thick rotatable steel inner liner inside a 1.5-in. thick steel vacuum tank. The bottom lid was welded to the vacuum tank. The top lid was bolted to the vacuum tank with six equiangularly spaced 3/4-in.-dia latch bolts and six 1-1/4-in.-dia SAE Grade 8 bolts.

The flywheel failure provided information that may be useful for flywheel containment specifications. The rotatable liner, whose I.D., O.D., and height were 30 in., 34 in., and 24 in., respectively, was broken into 12 fragments, whose fracture surfaces had the appearance of brittle failure. This fragmentation indicates that the primary stress pulse imposed by the failure fragments and particles on the rotatable liner exceeded its strength. The brittle fracture surfaces suggest that this failure was related to strain rate. Fragmentation of a rotatable liner is not acceptable if these fragments become projectiles. The six latch bolts were permanently deformed with one broken off its pin and tossed on the floor, and the 1 1/2-in. thick steel lid was deformed into six scallops at each latch bolt location. There was no failure of any of the larger 1-1/4-in. bolts. These deformations indicate that a significant axial pressure was generated as the failure fragments and particles rebounded off the rotatable liner and began secondary collisions with each other. One approach is to treat the failure fragments as a rotating fluid, which would cause the axial pressure to occur above and below the outer edge of the rotatable liner. The initial fix (not used in the Demo 1C test) was to place a deflecting flange at the top and bottom of the rotatable liner to direct this fluid back into the tank before it ever reaches the lid. A more uniform pressure on the lid results if the failure fragments are treated as elastically colliding particles that have rebounded from the rotatable ring. If this is the case, the initial fix may require a wider deflecting flange. Appendix A includes a more detailed discussion of the Demo 1C failure with analysis of the lower bound stress exerted on the rotatable liner by a disintegrating flywheel.

A three-step procedure will be used to propose innovative mobile automotive flywheel containment concepts grounded on ORNL's past test experience. First, test experience like that of the Demo 1C failure will be reviewed and used to help synthesize flywheel containment criteria. Second, the criteria will be attained using the strength of a thick-walled, steel cylinder. Finally, the specifications will be studied to see if they can be expressed through lightweight armor principles to provide a mobile containment capable of safely controlling the energy of a nominal 1.5 kW-h (5.4 MJ) automotive flywheel. Constraining requirements for the automotive containment are that it be small, light, and inexpensive.

Four of the considerations for designing a containment system are (1) the level of energy that must be controlled; (2) anticipated failure mechanisms, which depend on the flywheel and their effects on the containment; (3) available materials; and (4) methods of fabricating the shielding system. These considerations are discussed in the following sections.

4. FLYWHEEL ENERGY

Two types of energy are associated with the flywheel. The predominant energy is the kinetic energy; however, elastic potential energy is also stored because of the circumferential tensile stress and elongation during operation. The flywheel chosen for the calculations that appear in this paper consists of concentric cylinders pressed together. Their dimensions are chosen such that when they reach their intended speed the radial compressive stresses are negligible. The potential energy for this type of flywheel is easily calculated.

The equation for calculating the kinetic energy of a rotating cylinder is

$$K = 3.138 \times 10^{-8} \cdot \pi \cdot \frac{\rho}{g} \cdot \omega^2 \cdot h \cdot \left(\frac{R_o^4 - R_i^4}{4} \right) = 3.138 \times 10^{-8} \cdot \frac{M}{g} \cdot \frac{\omega^2}{2} \cdot \left(\frac{R_o^2 + R_i^2}{2} \right) \quad (1)$$

where

K is the kinetic energy, kWh;

ρ is the density, $\text{lb}_m/\text{in.}^3$;
 g is the gravitational constant, $386 \text{ lb}_m \text{ in.}/\text{lb}_f \text{ s}^2$;
 h is the height of the flywheel's rim, in.;
 R_i is the inner radius of the flywheel's rim, in.;
 R_o is the outer radius of the flywheel's rim, in.;
 ω is the angular velocity of the flywheel, rad/s ; and
 M is the mass of the flywheel's rim, lb_m .

The following calculations show that for a cylindrical flywheel the ratio of potential energy to kinetic energy for a rotating cylinder is the ratio of the ultimate strength to the elastic modulus. The equation for elastic potential energy is,

$$P = \frac{1}{2} \int \sigma \epsilon \, d\tau \quad (2)$$

where P is the elastic potential, in. lb_f ;
 σ is the circumferential stress in the flywheel, $\text{lb}_f/\text{in.}^2$; and
 ϵ is the circumferential strain in the flywheel, in./in.

The equations for circumferential stress and strain are,

$$\sigma = \frac{\rho}{g} \omega^2 r^2 \quad \epsilon = \frac{\sigma}{E} = \frac{\rho}{g} \frac{\omega^2 r^2}{E} \quad (3)$$

where

r is the radius (in.) of the flywheel at which the stress and strain are desired.

When the integral is taken over the flywheel rim from R_i to R_o and from 0 to 2π the result is

$$P = \frac{1}{2} \left(\frac{\rho}{g} \right)^2 \frac{\omega^4}{E} 2\pi h \frac{(R_o^6 - R_i^6)}{6} \quad (4)$$

The ratio of the potential energy to the kinetic energy of the flywheel is

$$\frac{P}{K} = \frac{\rho}{g} \frac{(\omega R_o)^2}{E} \frac{2}{3} \frac{\left[1 + \left(\frac{R_i}{R_o} \right)^2 + \left(\frac{R_i}{R_o} \right)^4 \right]}{\left[1 + \left(\frac{R_i}{R_o} \right)^2 \right]} \quad (5)$$

Since failure is expected when the peripheral stress equals the ultimate strength of the material from which the flywheel is constructed, it follows that the maximum value of this ratio occurs when R_i approaches R_o (a ring-like rim) and equals

$$\frac{P}{K} = \frac{\sigma_{ult}}{E} = \epsilon_{failure} \quad (6)$$

For materials commonly used in flywheels, the largest value is 0.04 for S-glass/ERL2258 composite. For T1000/ERL2258 the value is 0.017, for IM7/ERL2258 it is 0.016, for AS6/ERL2258 it is 0.014, for 300 maraging steel and titanium alloy it is 0.01, and for aluminum it is 0.007. The conclusion is that the elastic potential energy is only a small percentage of the total energy.

5. FAILURE MECHANISMS

Spin test experience published by companies, labs, and individuals participating in development of high-speed rotating components (1-13), data from the Demo 1C failure at ORNL, and discussions at the Flywheel Energy Storage Workshops held in Oak Ridge, Tennessee, in 1993 and 1995 provided a broad account of the types of failure mechanisms that must be addressed by designers of flywheel containment.

Though the type of failure mechanism depends mainly upon the flywheel design, other system components such as the motor/generator or bearing may have to be considered. The simplest flywheel design comprises a circumferentially wound composite rim mounted on a metal hub coaxially connected to a motor/generator with a bearing mounted metal shaft. If the bearings fail, a bumper surface may be used to constrain the shaft and flywheel until the energy is dissipated. If the shaft fractures, then the flywheel is free to orbit inside the containment and three severe failure events are possible.

First is the event in which strings of composite material from the flywheel pack between what remains of the rotating flywheel and the containment wall in such a way that the energy is too rapidly transferred to the bolts anchoring the containment to the vehicle. Fiberglass reinforced composites seem to be more prone to produce failure strings, often referred to as fluff. A commercial engineer said that no two places could be found in today's vehicles to which large enough anchor bolts could be secured that would survive such a packing failure. This is a severe failure mode that can be mitigated by a rotatable liner or by selecting a composite that does not produce failure strings.

Second is the event in which the metal hub fails and provides fragments that must not be allowed to breach the containment. It can be shown that a 133° sector of an annular fragment ejected from a rotating disk has maximum translational kinetic energy (11). This is the basis for the claim that a tri-hub burst is a worst case situation. Evaluation of the penetrating power of these fragments is the type of work that has been done in both the Uranium Separation Program and the Weapons Program at ORNL.

Third is the event in which the flywheel disintegrates into particles that produce a radial pressure pulse by elastically impacting the containment in the plane of the flywheel and then produce an axial pressure pulse by rebounding into collisions with outcoming out-of-plane particles. Recent experience by a flywheel developer with carbon fiber reinforced thermoplastic flywheels suggests that when this type of flywheel is released at speeds where the circumferential stress is 1/2 to 3/4 of its failure strength, its outer surface will abraid uniformly as it rubs down without disintegrating. The Demo 1C, whose rotor was carbon fiber reinforced composite, was

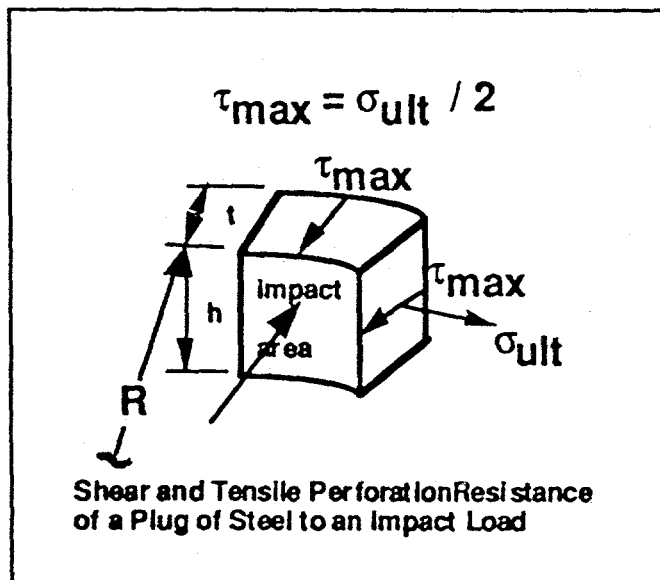
intentionally accelerated to ultimate burst failure; it failed at a speed where the circumferential stress was close to its ultimate strength and while spinning and orbiting in the bumper, sheared off the arbor and was projected against the wall of the liner where the impact caused it to disintegrate. There was no evidence of strings but only a layer of carbon dust on the inside of the rotatable liner.

The flywheel's motor/generator may be an integral part of the flywheel or it may be coupled to the flywheel through the shaft. If it is an integral part of the flywheel, then it may impose a dead weight load on the inner surface of the flywheel; this load must be considered as the flywheel is designed and tested. A shaft-coupled motor/generator may be the source of failure fragments, such as pieces of magnet, which must be controlled by the containment.

The more complicated polar wound flywheel design has radial fibers in addition to circumferential fibers. Because of their very high strength along the fibers, radial fibers, or bundles of radial fibers can act as rod projectiles. During the 1995 Flywheel Energy Storage Workshop, a representative from SatCon indicated that radial fibers from their record-breaking flywheel penetrated a 1-in. thick steel liner. This type of failure is similar to failure by penetrating hub fragments. Again, research in this area is similar to the military's blast, projectile, and shrapnel defeating problem.

The problem of matching radial growth at interfaces of rotating components appeared in an earlier series of experiments during which a common failure mode was separation of the rotor from the hub used to drive and support it. The basic physics for this occurs because rotating concentric rings of the same material grow away from each other as the rotational speed increases. This behavior is one of the major flywheel design challenges, which is to design for compatible radial growth at interfaces such as that between the shaft and hub or between the hub and the composite rim.

Any rotatable liner must resist perforation by fragments and destruction by pressure pulses. Design against perforation benefits from both tensile strength and shear strength properties of the liner material. Stage 1 of liner perforation is compression of the liner material over the impact area and shearing of material at the perimeter of the impact area (11). The shear strength of steel provides a significant contribution to successful perforation resistance.



If the ultimate shear strength is half the ultimate strength, then the pressure supported by a steel liner designed to resist perforation, neglecting strain rate effects, is

$$p = \frac{\sigma_{ult} \cdot t}{R} \left(1 + \frac{R}{h} + \frac{t}{2 \cdot h} \right) \quad (7)$$

where

R is the inner radius of the liner, in.,
 h is the height of the initial impact area, in.,
 t is the thickness of the liner, in., and

σ_{ult} is the tensile strength of the liner, (65 ksi for a typical liner).

The pressure equation may be solved for thickness as

$$t = (R + h) \cdot \left(\sqrt{1 + \frac{p \cdot 2 \cdot h \cdot R}{\sigma_{ult} \cdot (R + h)^2}} - 1 \right) \quad (8)$$

A methodology for estimating a lower bound of the pressure imposed on the liner by powder particles released from a flywheel which disintegrates as it impacts the liner ($b = 1.5$) is given in Appendix A. Evaluation of Eq. A.16 shows that for Demo 1C a maximum liner impact pressure occurs in the second quadrant. For $r = 12$ in. it is 159 ksi at 107° , for $r = 12.75$ in. it is 163 ksi at 114° , and for $r = 13.5$ in. it is 159 ksi at 122° . Furthermore, this pressure is 1.7 times greater than that produced by a concentric disintegration.

From Eq. 8, a perforation resistant A285 steel liner should have been 3.75-in. thick to withstand the estimated maximum 163 ksi pressure 114° from the point of impact in the Demo 1C disintegration at 1405 m/s.

Thicknesses were also calculated for perforation resistant liners of some cylindrical 1.5 kWh flywheels with various radii and lengths at a peripheral velocity of 1200 m/s. For pressures induced by central bursts, the liner thicknesses varied from 2.6 in. to 4.6 in. These thicknesses were further multiplied by 1.7 to resist perforation by pressures induced by eccentric bursts. These thicknesses produce liners that are too heavy for mobile use. Some relaxation of this design thickness may occur if Hagg and Sankey's energy equations are used. Their procedure considers stage 2, which is dissipation of energy by deformation of a plastic hinge on each side of the impact area. The hinges are three thicknesses long. It is clear that considerable work must be done to obtain a producible mobile liner that can withstand a radial pressure pulse from an eccentric disintegration.

The Demo 1C steel liner fractured brittly into 12 fragments suggesting that there is a strain-rate dependence of the liner's response to a pressure pulse. Figure 1 portrays the fragments projected onto the unrolled inner surface of the steel liner. A circumferential gouge near the plane of the flywheel centered on a triangular region burnished by axially moving particles identified the fragment that probably experienced initial impact. Even though the liner would need to be almost

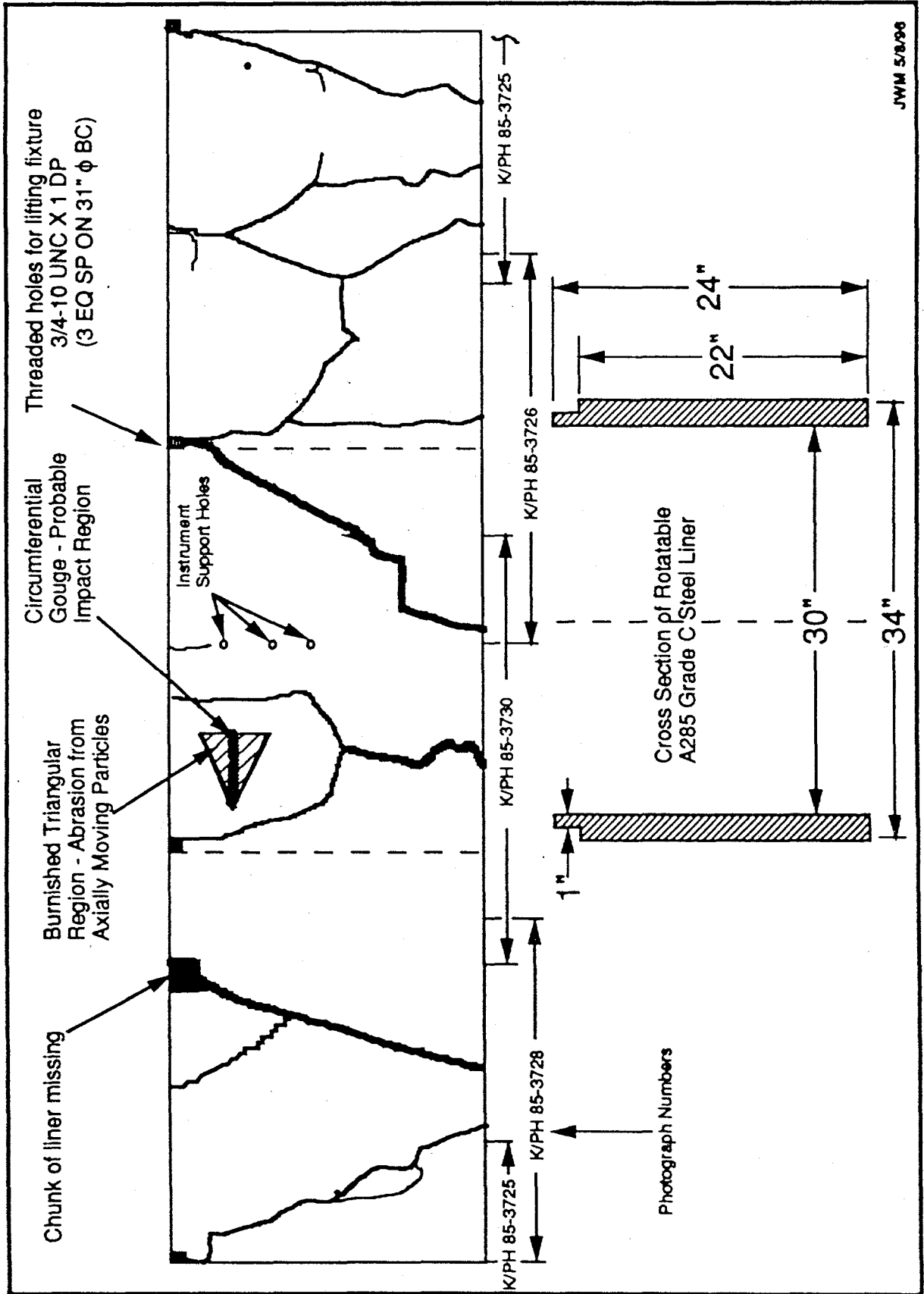


Fig. 1. Crack map for steel liner after failure of Demo 1C Flywheel

twice as thick to withstand the estimated maximum pressure of an eccentric burst using static material strength properties, the quantitative effect of strain rate effect is unknown. As part of the containment design effort, the strain-rate must be quantified before design criteria can be quantitatively applied. Note that the 1.5-in. thick wall of the tank was not damaged despite the liner being only 53% of the thickness estimated by Eq. 8.

6. LIGHTWEIGHT MATERIAL AND LAYERING CONTAINMENT CONCEPTS

There are possible remedies for each failure mechanism. One remedy for mitigating the effects of a wedge failure is a rotatable liner; however, the liner must not produce additional fragments as it resists penetration during exposure to flywheel fragments or to a pressure pulse. A remedy for preventing penetration of fragments from the hub or of bundles of radially oriented fibers may be selecting softer hub material or configuring the liner as a penetration shield. The problem of containing fragments and particles from a failed flywheel is analogous to the blast, projectile, and shrapnel defeating problem presented to the military. The military has two approaches; the first is to shatter the solid material and spread its energy; the second is to turn the solid material and spread its energy. Such a configuration might involve layering the liner with lightweight fiberglass or carbon fiber reinforced composites as a catcher at radii outside of disrupting layers such as stainless steel reinforced mat material, all outside of an inner cylindrical layer. Figure 2 depicts a schematic of a two layer example applied to both the rotatable liner and the outer housing. The material of the inner cylinder could be steel or ceramic depending upon what is required by analysis and demonstrated by testing. This type of research could benefit from ORNL's military shielding research. Activities to design safe containment for mobile hybrid flywheel systems should include a study of configurations of new lightweight composite materials and layering concepts.

Because of their high tensile strength along the fibers, lightweight fiberglass or carbon fiber reinforced composites might be configured to help resist radial pressure pulses and axial loads. This benefit is offset, however, by the low interlaminar shear strength of circumferentially wound composites. Axially oriented fibers could take advantage of the transverse fiber strength, which is above the interlaminar shear strength but still substantially below that of steel. Metal matrix composites, which have higher shear strength, could provide another design option.

7. FABRICATION AND ASSEMBLY

After materials with adequate properties are located and a containment has been proposed that satisfies the design criteria, the challenge remains to produce the flywheel module by enveloping the flywheel in the containment. Techniques must be developed to fabricate the layers needed on the liner to combat penetration and pressure pulses. The more layers required, the more complex this step will be. The most important assembly feature depends upon whether a requirement exists for repairability. If the module is a throwaway, then the upper and lower housing may be welded together over the flywheel. This will produce a less expensive unit that is better hardened against axial pressure pulses. If the module must be repairable, then it must be possible to separate the two halves. This might be accomplished by bolting them together; however, such a configuration, although cheaper, requires mating flanges that will increase the overall diameter of the housing and is much weaker against axial pressure pulses. A more likely configuration would be to screw them together as shown in Fig. 2. Once the housing halves are connected, a technique must be developed to overwind any additional support. If the overwinding is one piece, it must be destroyed before the module may be disassembled for repair. If it is in two pieces, it will provide no additional support against axial pressure pulses.

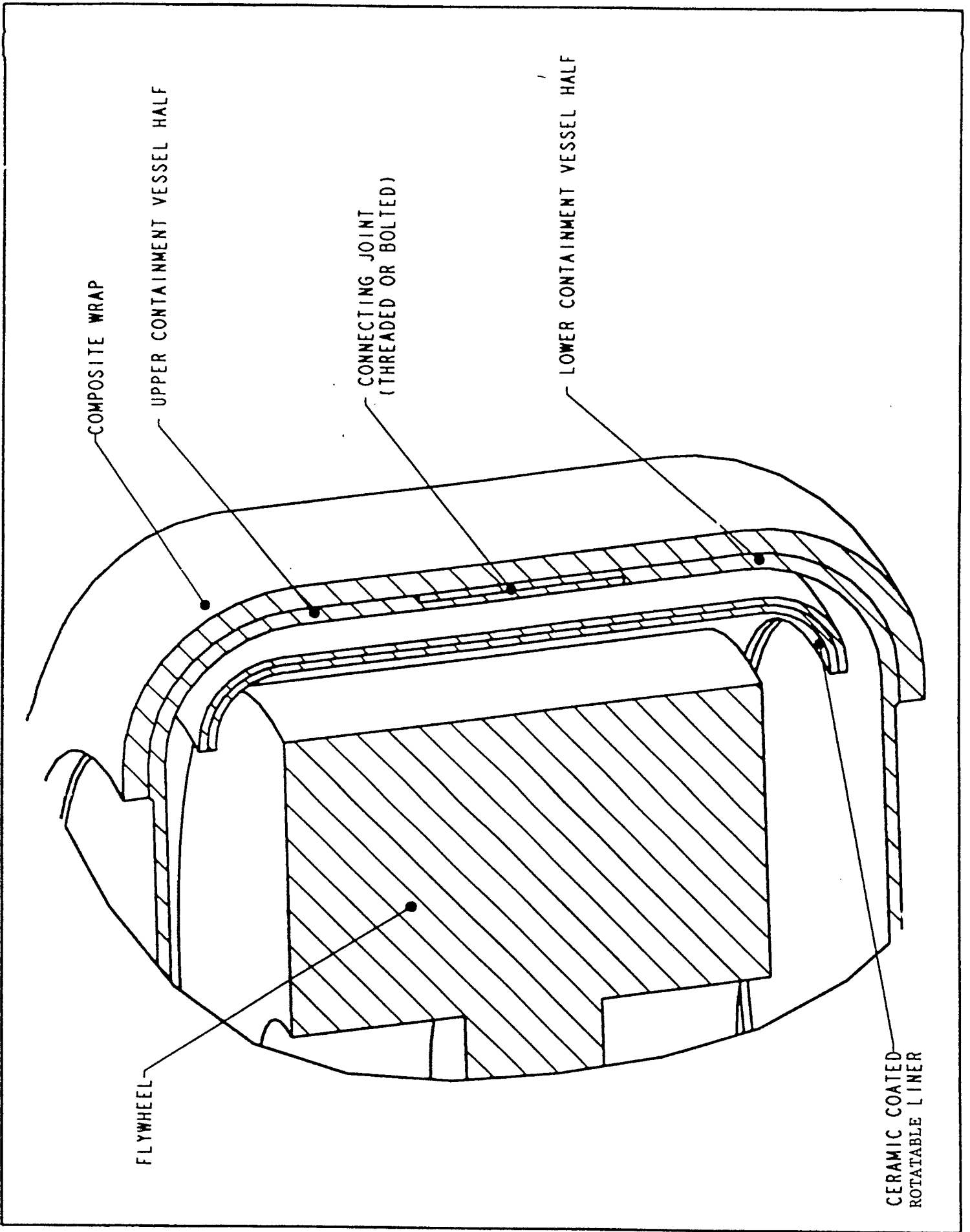


Fig. 2. Flywheel containment detail.

Lightweight materials, some of the disrupter materials, and ceramics tend to be expensive. The design challenge will be to minimize the use of expensive materials while obtaining the necessary benefits and to invent fabrication techniques that permit cost effective fabrication and assembly of the flywheel module.

8. CONCLUSIONS

This section presents the conclusions from the investigations, discussions, analyses, and calculations related to this laboratory directed research on flywheel containment.

1. The flywheel failure mechanisms depend strongly on the flywheel design, thus safe containment will vary from design to design.
2. A rotatable liner may be an attractive approach to combat a packing failure, but it must be designed so that it is perforation resistant and does not produce secondary fragments. Packing failures occur when the failing composite produces strings that bunch up to create a packing nest. It may be possible to avoid packing failure by selecting a composite that fails as dust rather than strings. Allowing the entire housing to rotate is another approach to extend the time during which torque is transmitted to the mounting structure.
3. The shear strength of the liner is even more important than its tensile strength in resisting perforation by fragments and pressure pulses. This feature will make it challenging to meet liner design requirements with lightweight materials whose interlaminar and transverse shear strengths are characteristically low.
4. The estimated pressure pulse on the liner from inelastic collisions of the disintegrating particles is a lower bound. Inelastic collisions do not predict an axial pressure which was sufficient to deform five of the lid bolts in the Demo 1C failure and fracture the sixth. This shows that the collisions are partially elastic. Since elastic fragment collisions deposit twice the momentum on the liner wall, a blind estimate of maximum pressure is twice the value produced by inelastic collisions if the time of the elastic collision is the same as the time of crushing during an inelastic collision; however, secondary elastic collisions of particles elastically rebounding from the liner with outcoming particles not in the same plane will prevent a significant number of primary liner collisions, which in turn could significantly reduce the maximum pressure pulse. A model is needed that can predict development of both the radial and axial pressure pulses.
5. Concentric disintegration of a flywheel produces a uniform pressure on the liner. Eccentric disintegration produces a circumferentially varying pressure profile with a maximum about 114° from the point of impact with the liner. The maximum pressure pulse from the eccentric disintegration is about 70% greater than that produced by concentric disintegration.

9. RECOMMENDATIONS

Recommendations for future research related to flywheel containment are the following:

1. Explore containment configurations that use new lightweight composite materials, metal matrix composites, and layering concepts. Review ORNL's research on

the blast, projectile, and shrapnel defeating problem to see what may be applied to solve the flywheel fragment penetration problem. Explore different configurations of composite materials to see if overwrapping the liner and/or the housing can provide any benefit to resist penetration and separately to withstanding disintegration pressure pulses.

2. Continue efforts to determine what radial pressures must be withstood by the rotatable liner recognizing that the radial pressure estimates given in this paper are lower bounds which could be considerably higher for elastically rebounding failure particles. A time delay occurs between collision of the flywheel with the liner and a later time that the impact pulse induces disintegration at a point in the rotating flywheel. Calculate the effect of this delay on the circumferential pressure distribution of an eccentric failure.
3. Quantify the strain-rate effect at the 27- to 54-per-second level so that it may be used to design perforation resistant rotatable liners. This will require a carefully designed test program coordinated to obtain material constants that reflect strain rate. Inquire to see if the sophisticated equipment required for this testing is available at ORNL.
4. Develop a model that will simulate formation of the radial and axial pressure pulse based upon the failure fragment sizes and the coefficient of restitution of these fragments with the liner and with each other. Coordinate test instrumentation to verify the model. This information will be useful for designing the radial and axial geometry of the rotatable liner.

10. REFERENCES

1. C. R. Keckler, R. T. Bechtel, and N. J. Groom (eds.), "An Assessment of Integrated Flywheel System Technology," *NASA Conference Publication 2346*, November 1984.
2. R. S. Steel, Jr., J. M. Casstevens, and B. J. Sutton, *Oak Ridge Flywheel Evaluation Laboratory Annual Report, Y-2210*, December 1979.
3. R. S. Steel, Jr., *Oak Ridge Flywheel Evaluation Laboratory Qualification Review, Y/DX-100*, January 1980.
4. R. S. Steel, Jr. and E. F. Babelay, Jr., *Data Analysis Techniques Used at the Oak Ridge Y-12 Plant, Y/DX-185*, August 1980.
5. R. S. Steel, Jr. and E. F. Babelay, Jr., *Test Results for William M. Brobeck and Associates, Y/DX-185*, August 1980.
6. R. S. Steel, Jr. and E. F. Babelay, Jr., *Composite Flywheel Testing and Evaluation at the Oak Ridge Flywheel Evaluation Laboratory, Y/DX-202*, October 1980.
7. R. S. Steel, Jr., E. F. Babelay, Jr., and B. J. Sutton, *Rockwell-Rocketdyne Flywheel Test Results, Y/DX-244*, January 1981.
8. R. S. Steel, Jr. and E. F. Babelay, Jr., *Oak Ridge Flywheel Evaluation Laboratory Test Report on the Garrett Airesearch Flywheel, Y/DX-227*, February 1981.
9. R. S. Steel, Jr., *Composite Flywheel Balance Experience, Y-DX-290*, April 1981.

10. R. S. Steel, Jr., E. F. Babelay, Jr., and B. J. Sutton, *Hercules Aerospace Flywheel Test Results*, Y/DX-319, June 1981.
11. A. C. Hagg and G. O. Sankey, "The Containment of Disk Burst Fragments by Cylindrical Shells," pp. 114-123 in *Transactions of the ASME*, April 1974.
12. H. E. Sonnichsen, "Ensuring Spin Test Safety," pp. 72-77 in *Mechanical Engineering*, December 1993.
13. A. P. Coppa, *Composite Ring-Disk Flywheel Design, Fabrication, and Testing*, Document No. 83SDS4248, General Electric, Space Systems Division, August 1983.
14. R. Chuse, *Pressure Vessels: The ASME Code Simplified*, Fifth Edition, McGraw-Hill, 1977.
15. *Flywheel Energy Storage Technology Workshop*, November 2-4, 1993, Oak Ridge, Tennessee, Conference 9311155.
16. *Flywheel Energy Storage Technology Workshop*, October 31-November 2, 1995, Oak Ridge, Tennessee, Conference 9510242.

APPENDIX A

REVIEW OF THE DEMO 1C FLYWHEEL TEST

On December 9, 1985, the flywheel known as Demo 1C shown in Fig. A.1 was spun to failure in a top loading spin tank at the ORNL flywheel test facility. The spin tanks are located in a reinforced concrete revetment area shown in Fig. A.2 at the K-25 plant in Oak Ridge, Tennessee. The flywheel rim comprised two concentric circumferentially wound carbon fiber reinforced cylindrical rings whose total weight was 6.2 kg. The inner ring was AS6 and the outer ring was IM6. The rings were mounted on a metal hub, which in turn was connected through an arbor to the quill of the 4-in.-dia air turbine used to drive the flywheel to failure. Failure occurred at 1405 m/s at which point the energy in the rim was 1.5 kWh. This is the energy being considered for use in load levelers capable of extending the range of automobiles by up to 30%.

FLYWHEEL SPIN TEST SYSTEM

Configuration

A schematic of the spin tank is shown in Fig. A.3. The A 285 Grade C steel vacuum casing consists of a 1-1/2-in. thick cylinder with a 35 3/8-in. ID welded to a 1-1/2-in. thick annular region of its bottom disk and bolted during operation through a 1-7/8-in. thick region of its removable top disk. The bottom disk is bolted with 16 1-in. dia SAE Grade 8 bolts on a 42 1/2 in.-dia bolt circle to the flange of a 12-in. high spool piece. The spool piece is anchored in the concrete floor with 16 1-in. dia bolts. Six 3/4-10 latch screws made of 4140 steel and six 1 1/4-7 SAE Grade 8 bolts secure the top lid to the vacuum cylinder. Each latch screw is held by a 3/4-in. dia rod pressed into a steel fixture welded to the outside of the vacuum cylinder. The elongation length of each 3/4-in. bolt is 4 in. Each 1-1/4-in. bolt passes through a hole in the lid and a 4-in. steel cube welded to the side of the vacuum cylinder. The elongation length of each 1-1/4-in. bolt is 7.5 in. A 24 in. high 2-in. thick inner liner with a 30-in. ID is mounted on spacers to allow it to rotate if impacted during testing. A 2-in. high collar with a 33-in. ID and a 35-in. OD sits on the top of the rotatable liner to prevent it from tilting into the ID of the vacuum cylinder. The flange of the air turbine is secured to the top of the lid with four 3/8-16 bolts on a 4-in. bolt circle threaded 3/4 in. into the lid.

Bumper Bearing

A steel cylinder with an internal brass bearing surface is bolted concentric to the turbine quill with six 1/2-13 SAE Grade 8 bolts on a 6-in. dia bolt circle in a 1/2-in. deep recess inside the lid. This is a bumper bearing, which serves as an arbor runout delimiter and is shown in Fig. A.4. The brass surface provides a rubdown surface for the 2-in. OD of the top of the arbor, which is mounted on the turbine quill and held in place with three Allen-head screws. One of the holes through which the screws are tightened is visible in Fig. A.4, along with what remains of the arbor. If the eccentricity from a sudden imbalance exceeds 0.060 in. during operation, the arbor touches and orbits on the ID of the brass cylinder. Often the assembly may be brought to rest without further failure, thus enabling visual analysis of what caused the imbalance.

Arbor

This arbor was made of aluminum. It had three parts which, from top to bottom, are the 2-in.-dia cylinder into which the 5/16-in.-dia turbine quill is inserted, the runout cylinder, and the 5/8-in.-dia threaded shank. The shank is inserted with interference through the bore of the flywheel's hub and secured with a nut and Belleville washer. In Fig. A.4, the entire shank is missing although the runout cylinder is still intact.

Failure Scenario

The failure of the flywheel, which occurred at a peripheral velocity of 1405 m/s (38,650 rpm), was dramatic. During the first event, which lasted for about three seconds, the 2-in.-dia top cylinder of the arbor orbited on the inner bearing surface of the bumper bearing. The second event was a loud crash followed by a cloud of carbon dust rising from the revetment cubicle. The dust exited from the spin tank at the joint between the tank and the lid. Figure A.4 suggests that the huge shearing forces from the imbalanced flywheel orbiting inside the bumper bearing caused it to shear off the arbor just below the runout cylinder. An estimated orbiting frequency of 1396 rad/s, or 222 Hz, is sufficient to generate the required shear load. If the flywheel sheared off the arbor at this angular velocity, it would reach the liner in about 0.01 s (long before it reached the floor of the tank). The shank of the arbor, which was ripped from the hub during failure, was retrieved from the debris in two pieces along with the Belleville washers and the nut. The nut was still attached to one piece of shank as shown in Fig. A.5. The loud crash was probably the flywheel rim striking the inner liner with such impact that it caused the flywheel to shatter. An audio recording of the events and a visual recording of the movement of the tank's top lid, which showed amplified motion at the top of the three-foot long turbine muffler mounted on the axis of the turbine with dust billowing out around the edges, provides a lucid external picture of what happens during a disintegration type of failure.

The scene is shown in Fig. A.6 after the dust settled. Metal fragments from the hub had eroded the revetment wall in the plane of the top lid and dust from the carbon fibers stenciled an image of the opening formed by the deflected lid (see Fig. A.7) during its response to the pressure pulse from the disintegrating flywheel. The six 3/4-in. latch bolts were stretched or broken and Fig. A.5 shows one that had been thrown from the tank. Numerous electrical and instrumentation cords had been severed or stripped by particles escaping the tank. Figure A.8 shows carbon and epoxy powder coating the inner liner and packed between the lid and the casing. No strands of carbon fiber or fluff remained.

Radial Pressure Pulse

The response of the 2-in. thick liner to the radial pressure pulse from the flywheel failure is significant. The liner was shattered into 12 fragments. Figure A.9 shows four of these fragments. Their fracture surfaces all have the granular appearance of a brittle fracture. The liner must conform to A 285 Grade C steel, which has an ultimate strength of 55 to 75 ksi, and an elongation to failure in 2 in. of 27%. The hardness of one of the fragments was checked and indicated that the material properties were acceptable. The conclusion is that the strain rate capabilities of this material were exceeded, which means that the very short high-pressure pulse exceeded the material strength values that are different than the quasi-static properties given in the literature. The last section of this appendix presents a method for estimating the lowest pressure that will be exerted on the inside of the liner by a disintegrating flywheel like Demo 1C.

Axial Pressure Pulse

From the response of the rotatable liner, one can understand why accommodating the radial pressure pulse receives significant attention during preparation for a high-speed rotation test. Demo 1C clearly indicated an axial pressure pulse that was high enough to elastically deform five latch bolts and fracture one and to scallop the edge of the thick steel lid. Figure A.5 shows the latch bolt that had been thrown to the wall of the revetment after its eye had fractured.

Observations of deformation or absence of it in the six 3/4-in.-dia 4140 steel latch bolts, in the remaining six 1-1/4-in.-dia grade 8 steel bolts, and in the A285 steel lid may support an estimate of the maximum upward force exerted on the lid during failure. Figure A.6 shows that

only one of the latch bolts remained upright after the failure. Four of the other bolts had elongated sufficiently that they could be rotated out of the radial slot by debris escaping the tank or by vibration. The eye of one latch bolt (Fig. A.5) failed where the stress concentration factor is 2.8 thereby indicating the presence of a defect. Although the bolts have been discarded observers indicated that the large bolts had behaved elastically. Because of the stress concentration factor of 3.8 at the first engaged thread, one would expect plastic yield to occur at the root diameter for a load, P, of

$$P = \frac{\sigma_y A_T}{K_T} \quad , \quad (A.1)$$

where

σ_y is the yield stress of the bolt, 150 ksi,
 A_T is the area of the thread for tensile failure, .969 in.², and
 K_T is the stress concentration factor for threads, 3.8.

If in fact no yielding occurred at the thread notch, then the load on each grade 8 bolt did not exceed 38,000 lbs. Each of the latch bolts was permanently deformed indicating an ultimate bolt load of 55,778 lbs. The estimated total upward force resisted by 12 bolts under this assumption is 563,000 lbs. Further finite element modeling or potential energy minimization for the lid/bolt system should be completed to more exactly determine the load distribution on the bolts.

Axial Pressure Lower Bound Estimate

Some current thinking is that the axial pressure pulse is applied to the lid in an annular region as the flywheel particles deflect upward, thereby affecting the upward load on the lid. The equation for the pressure that will produce an upward load of 563 thousand pounds is a function of the annular OD and ID. It is given by the equation

$$P = \frac{471.3}{1 - \left(\frac{ID}{OD}\right)^2} \quad , \quad (A.2)$$

where

OD is the diameter of the O-ring that seals the tank, 39 in., and
 ID is the inner diameter of the annular region, in.

If ID is zero, the pressure is uniformly applied to the entire lid and is 1004 psi. For a 2-in.-wide annular region with ID=35 in., the pressure is 2422 psi. Remember that the actual pressure is probably higher because of the relief provided by the gap formed as the lid stretches the bolts.

Estimate of Radial Pressure on the Rotatable Liner

There is disagreement about the necessity of a rotatable liner. One concern is that if the inner liner fails it may provide secondary fragments to increase the penetration probability and amplify the reaction of the containment to the breakup. In ORNL's experience, rotatable liners

have effectively absorbed kinetic energy of typical failures, defined as those operational failures that occur well below the ultimate strength of the flywheel material. It will be important, however, to assure that any rotatable liner design will mollify the action of secondary fragments. This may be accomplished by employing new types of lightweight composite material to provide a layered rotatable liner hardened against particular types of failure reactions.

Three types of failure reaction are prominent. The first is the reaction of the liner or vacuum jacket to the initial impacts of flywheel system fragments formed during failure. Undesirable reactions are fragmentation or penetration. ORNL's Demo 1C provided an example of liner fragmentation. Both ORNL and the flywheel development community have had experience with penetration by metal fragments and by carbon fibers in a longitudinal arrow-like orientation. The second is the reaction of the ends of the liner extensions and vacuum jacket to all post primary impacts of flywheel system fragments. These post primary impacts can induce a significant axial load. The third is the reaction of the containment when the flywheel failure debris suddenly wedges internally causing a very high torque on the bolts holding the jacket to the mount frame. This type of wedging may be expected for fiberglass reinforced composites because of their higher transverse strength, but may not be common for carbon fiber reinforced composite because of the brittleness of carbon fiber.

Material selection and a rotatable liner may take care of the packing reaction by eliminating packing strings and fluff the fragment axial reaction will be the subject of some future modeling to understand how and where it is applied so that it may be most effectively controlled, but understanding the fragment radial reaction may be crucial to developing a safe, low-cost, mobile containment. The Demo 1C failure provided information that has improved our understanding of the fragment radial reaction. A likely scenario of its failure is that the radial pressure pulse was generated as minute flywheel particles impacted the liner. These minute particles were formed when the flywheel was shattered after it sheared off the arbor and laterally struck the liner. The derivation that follows estimates the lower limit of the pressure on the liner that would be caused by inelastic collision of a very large number of minute (powder) particles.

Repeated reference is made to minute particles because their size must be small to neglect the contribution to angular momentum of their rotation. When a rotating system breaks into multiple fragments, the angular momentum may be expressed with two terms. The first term contains the translational velocity of each fragment tangent to the radius through its center of mass, and the second term contains angular rotation of the fragment about its center of mass. This angular rotation is equal to the system's angular rotation prior to breakup. It can be shown that, as the number of fragments increases and the corresponding particle size approaches zero, the ratio of the angular momentum due to rotation of the fragments divided by the angular momentum due to translation of the fragments approaches zero. That is, for a flywheel that disintegrates into powder, conservation of angular momentum is satisfied by translation of the powder particles.

Assumptions

There are four assumptions upon which the radial pressure estimate is based for the Demo 1C failure scenario.

1. Centripetal loading from the flywheel on the aluminum arbor as it eccentrically orbited inside the bumper bearing caused the flywheel to shear the arbor shaft below the runout cylinder and strike the rotatable liner, instantly disintegrating.
2. The disintegration produced an infinite number of infinitely small particles that were released to travel perpendicular to their radii at the instant of disintegration with a velocity, ωr .

3. The impact of each particle with the rotatable liner is inelastic. For an inelastic collision each particle will impact the liner and stick. The change in momentum is $mv - 0 = mv$. Recall that this is half the momentum change for an elastic collision, which is $mv - (-mv) = 2mv$; consequently, the pressure from the actual collision will be larger than for the inelastic collision. From the outside to the inside of the flywheel there is a locus of particles that all impact the same point on the liner. Since each particle sticks to the liner in an inelastic collision, the path is clear for impact of another radially inward particle to strike the liner. There is a unique locus for each impact point on the liner. That locus lies on the intersection of the flywheel and the semi-circle whose diameter is the distance from the center of the flywheel ($b, 0$), to the impact point (x_1, y_1). Inelastic collisions generate no axial load because all the particles stick to the liner.

Axial motion may be imparted to disintegrated particles from rebound of their axial Poisson contraction. This contraction occurs as the impact wave travels through the flywheel releasing the tensile stress by causing disintegration of the flywheel material. Axial momentum is generated by particles rebounding from the liner to collide with oncoming particles. The axial load on the lid comes from the axial momentum produced by these out-of-plane collisions.

Here is the procedure for estimating the pressure exerted on the liner at (R, α) by each particle from a disintegrated flywheel whose axis is displaced from the center of the liner by distance, b . Figure A.10 is a schematic of the variables and geometry used in this derivation.

The coordinates of the impact point are given by

$$x_1 = R \cdot \cos(\alpha) \text{ and } y_1 = R \cdot \sin(\alpha). \quad (\text{A.3})$$

The distance from the center of the flywheel to the impact point is

$$c = \sqrt{R^2 + b^2 - 2 \cdot R \cdot b \cdot \cos(\alpha)}, \quad (\text{A.4})$$

where b is the distance from the center of the rotatable liner to the center of the flywheel.

The polar angle of the impact point with respect to the center of the flywheel is

$$\zeta = \arccos\left(\frac{x_1 - b}{c}\right) \cdot \frac{y_1}{|y_1|}, \quad (\text{A.5})$$

where the value of y_1 divided by its absolute value accounts for function sign changes between quadrants.

The tangential velocity of a particle at radius, r , is

$$v = \omega \cdot r, \quad (\text{A.6})$$

where ω is the angular velocity of the flywheel, 4097 rad/s.

The angle between c and the trajectory of the disintegrated particle is obtained using the law of sines and is

$$\kappa = \text{asin} \left(\frac{r}{c} \right). \quad (\text{A.7})$$

The angle between c and flywheel radius of the disintegrated particle is

$$\eta = \frac{\pi}{2} - \kappa. \quad (\text{A.8})$$

The polar angle of the disintegrated material with respect to the center of the flywheel is

$$\theta = \zeta + \eta = \zeta + \frac{\pi}{2} - \kappa. \quad (\text{A.9})$$

The cartesian coordinates of the disintegrated particle are

$$x_3 = b + r \cdot \cos(\theta) \quad \text{and} \quad y_3 = r \cdot \sin(\theta). \quad (\text{A.10})$$

The distance from the center of the tank to the disintegrated particle is

$$f = \sqrt{x_3^2 + y_3^2}. \quad (\text{A.11})$$

The distance from the impact point to the disintegrated particle is

$$e = \sqrt{(x_1 - x_3)^2 + (y_1 - y_3)^2}. \quad (\text{A.12})$$

The angle of incidence of the impacting particle on the liner is

$$\tau = \text{acos} \left(\frac{e^2 + R^2 - f^2}{2 \cdot e \cdot R} \right). \quad (\text{A.13})$$

The value of $dc/d\alpha$, which is used to calculate $d\theta/d\alpha$, is

$$\frac{dc}{d\alpha} = \frac{R \cdot b \cdot \sin(\alpha)}{c}. \quad (\text{A.14})$$

The value of $d\theta/d\alpha$, which is used to calculate the pressure generated by the particle, is

$$\frac{d\theta}{d\alpha} = \left[\frac{(R \cdot \cos(\alpha) - b) \cdot \frac{dc}{d\alpha} + c \cdot R \cdot \sin(\alpha)}{c \cdot c^2 - (R \cdot \cos(\alpha) - b)^2} \right] \cdot \frac{y_1}{|y_1|} + \frac{r \cdot \frac{dc}{d\alpha}}{c \cdot c^2 - r^2} \quad (\text{A.15})$$

The estimated pressure in psi exerted on the liner at the impact point is

$$\sigma = \frac{dF_{\perp}}{dA} = \frac{\rho}{g} \cdot \frac{r}{R} \cdot (v \cdot \cos(\tau))^2 \cdot \frac{d\theta}{d\alpha} \quad (\text{A.16})$$

The time required for the disintegrated particle to reach the liner is

$$t = \frac{e}{v} \quad (\text{A.17})$$

The torque per radian exerted on the liner as a function of α is

$$\Delta t = \frac{dr}{v \cdot \cos(\tau)} \quad (\text{A.18})$$

The equation for the radial load from an incoming particle is estimated as the change in radial momentum of the particle during its inelastic collision divided by the time over which this momentum change occurred. The stress is the load divided by the area of the liner over which the load is imparted. The mass of the particle is

$$dm = \rho \cdot r \cdot d\theta \cdot dr \cdot h, \quad (\text{A.19})$$

and the change in radial momentum for an inelastic collision is

$$dp_{\perp} = \frac{dm \cdot v \cdot \cos(\tau)}{\Delta t} \quad (\text{A.20})$$

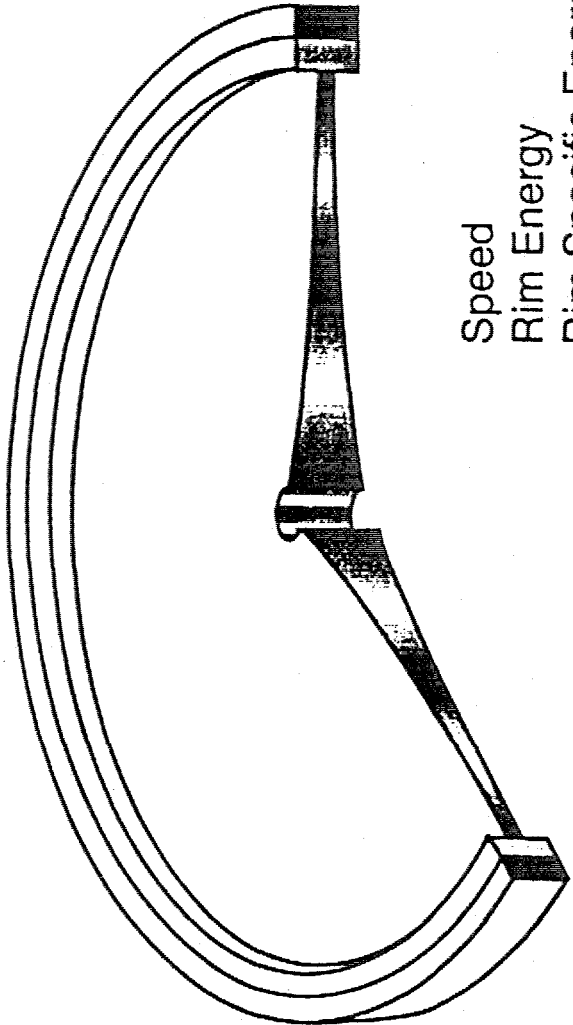
The time over which the momentum change occurs is estimated as

$$dF_{\perp} = \frac{\rho}{g} \cdot r \cdot d\theta \cdot h \cdot (v \cdot \cos(\tau))^2 \quad (\text{A.21})$$

The radial force on the liner is then

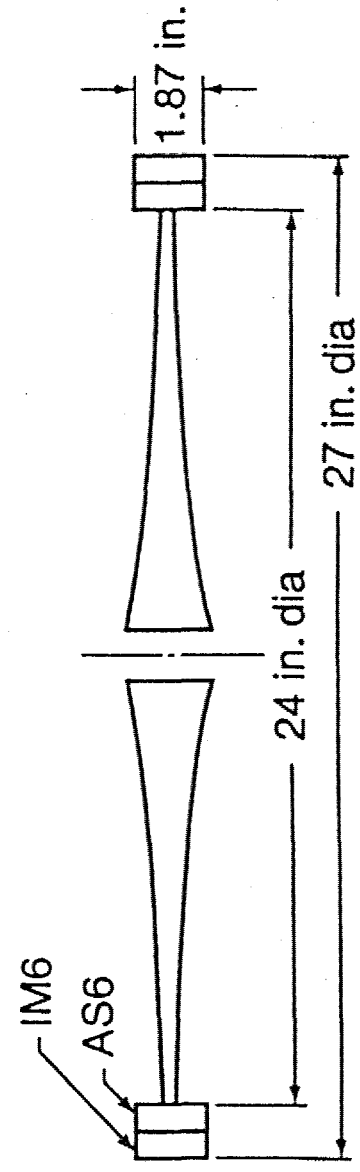
$$\frac{dT(\alpha,r)}{d\alpha} = \sigma(\alpha,r) \cdot R^2 \cdot h \cdot \tan(\tau) \quad (\text{A.22})$$

The load is distributed on the liner over area, $hR d\alpha$, leading to the stress at the impact point given by Eq. A.16 above.



DEMO 1C

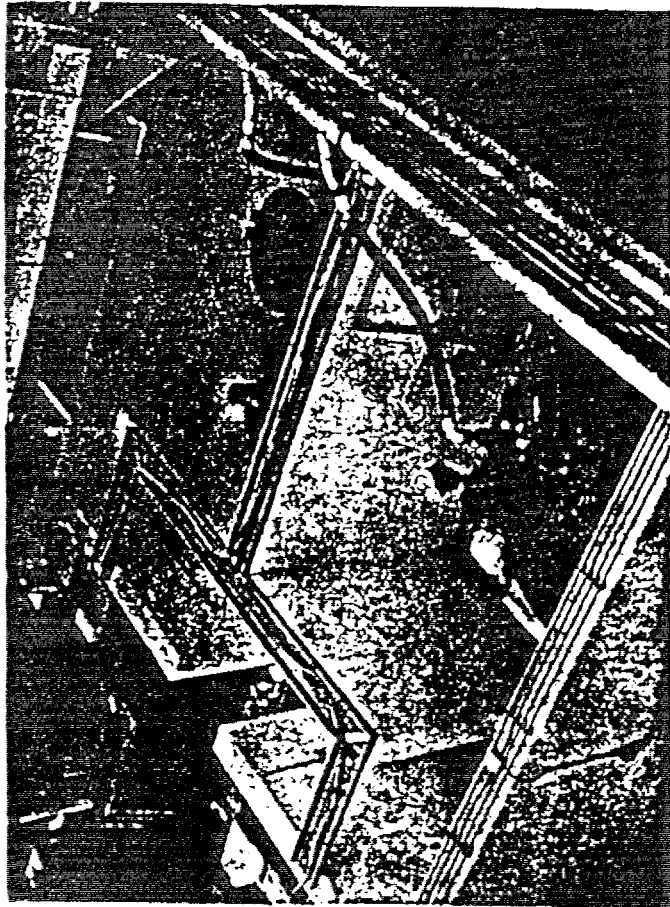
Speed	1405 m/s
Rim Energy	5.45 MJ (1.51 kWh)
Rim Specific Energy	878 kJ/kg (244 Wh/kg)
Total Energy	7.28 MJ (2.02 kWh)
Total Specific Energy	420 kJ/kg (117 Wh/kg)
Date:	December 9, 1985



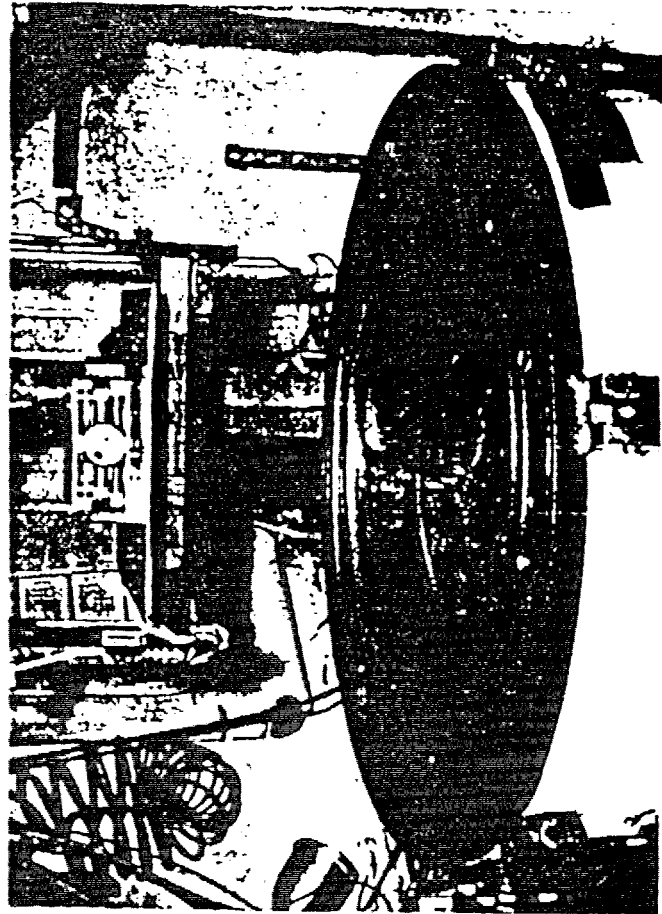
D.U. O'Kain
oml

Fig. A.1. High speed flywheel demonstration.

AIR TURBINES WHICH ARE USED FOR HIGH-SPEED TESTING; ENCLOSED IN A REINFORCED CONCRETE REVETMENT AREA



AIR TURBINE TANK WITH ROTATING ENERGY-ABSORBING LINERS



MARTIN MARIETTA

Fig. A.2. High speed rotational testing.

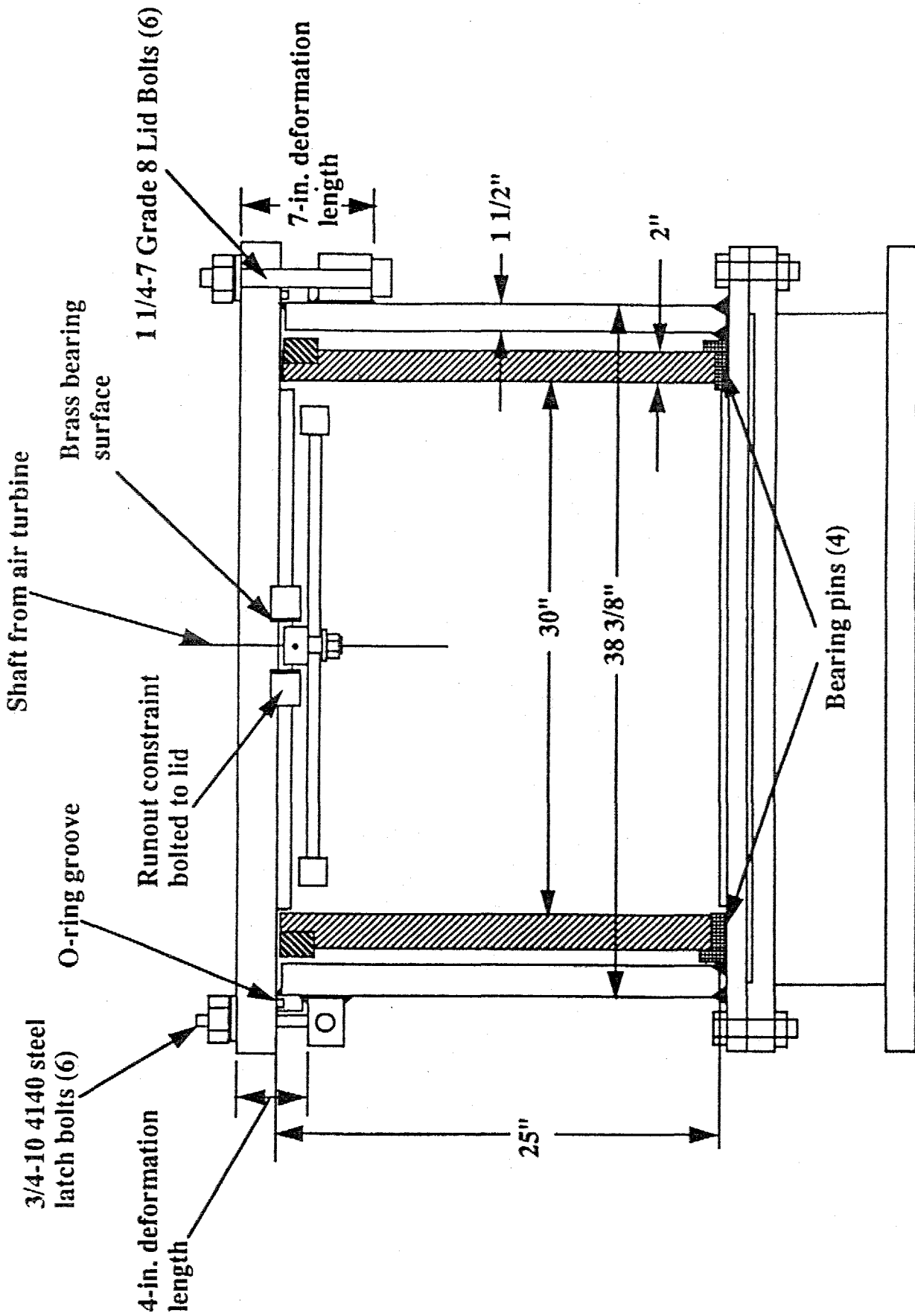


Fig. A.3. Schematic of spin tank in which DEMO 1C was tested.



Demo 1C - Something's Missing

ornl

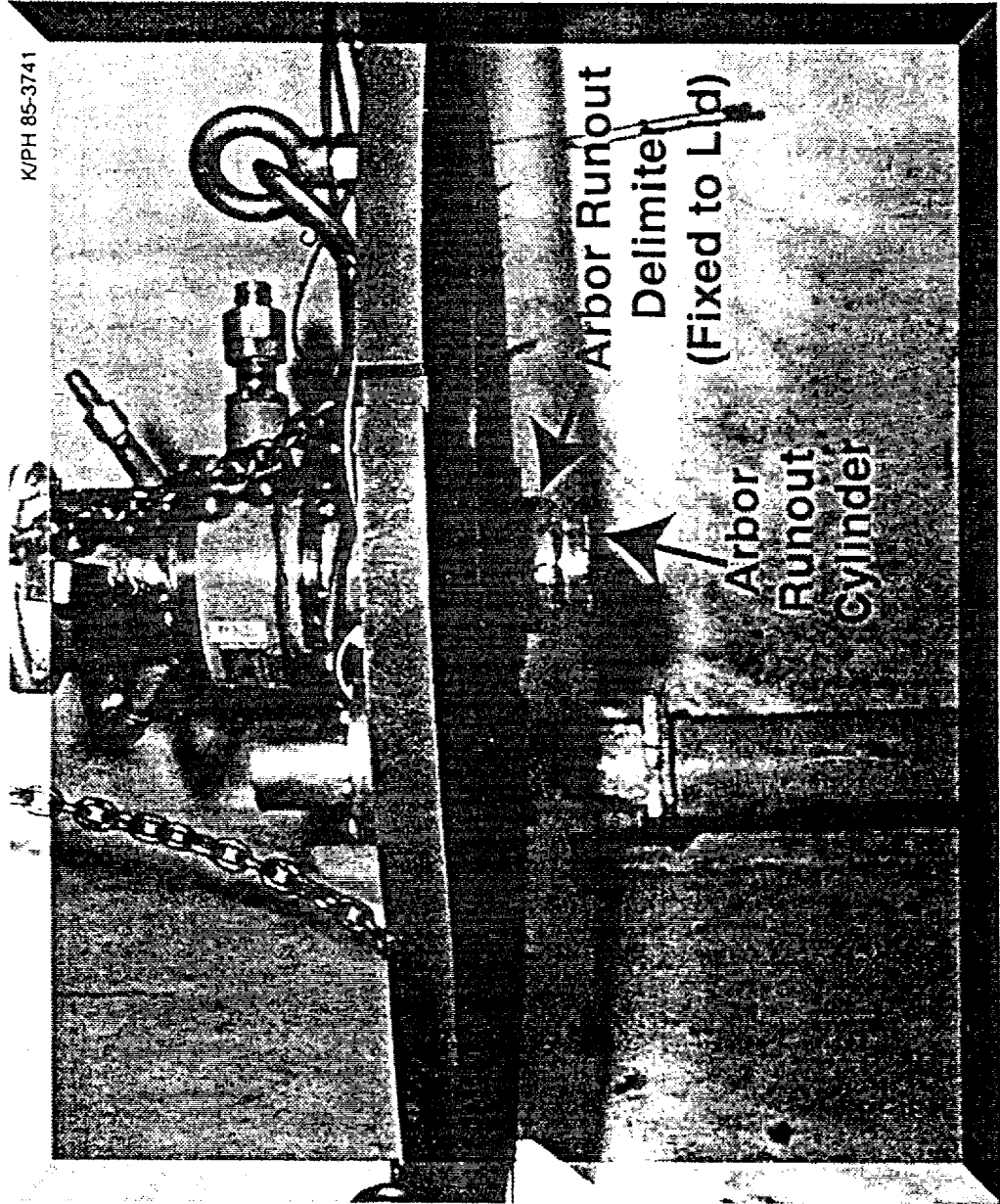
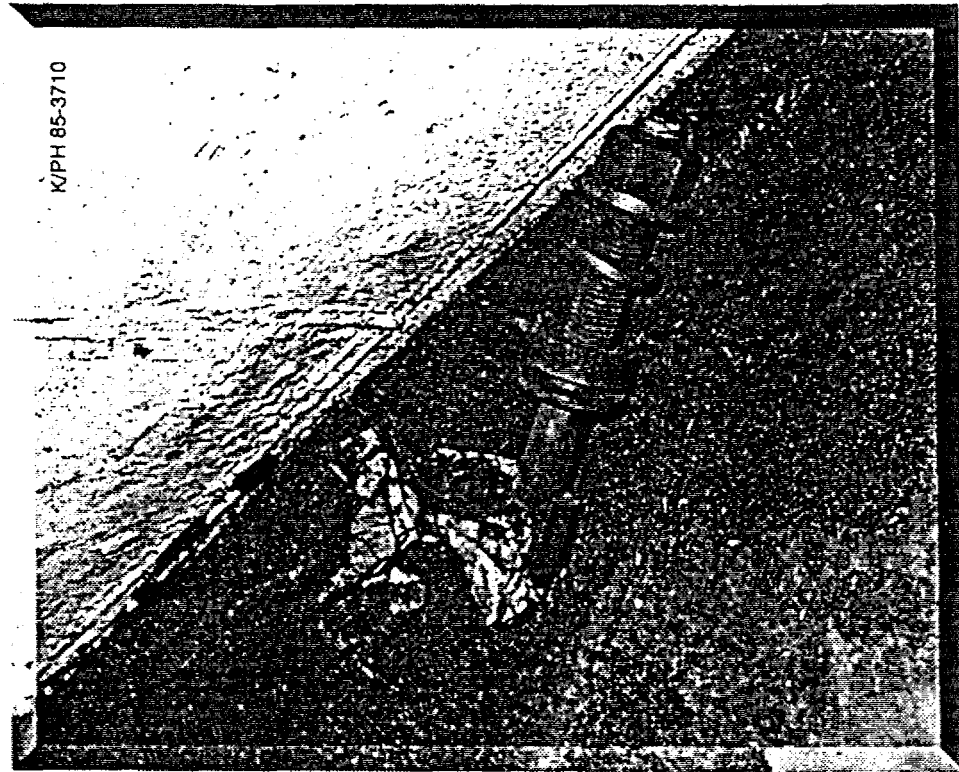


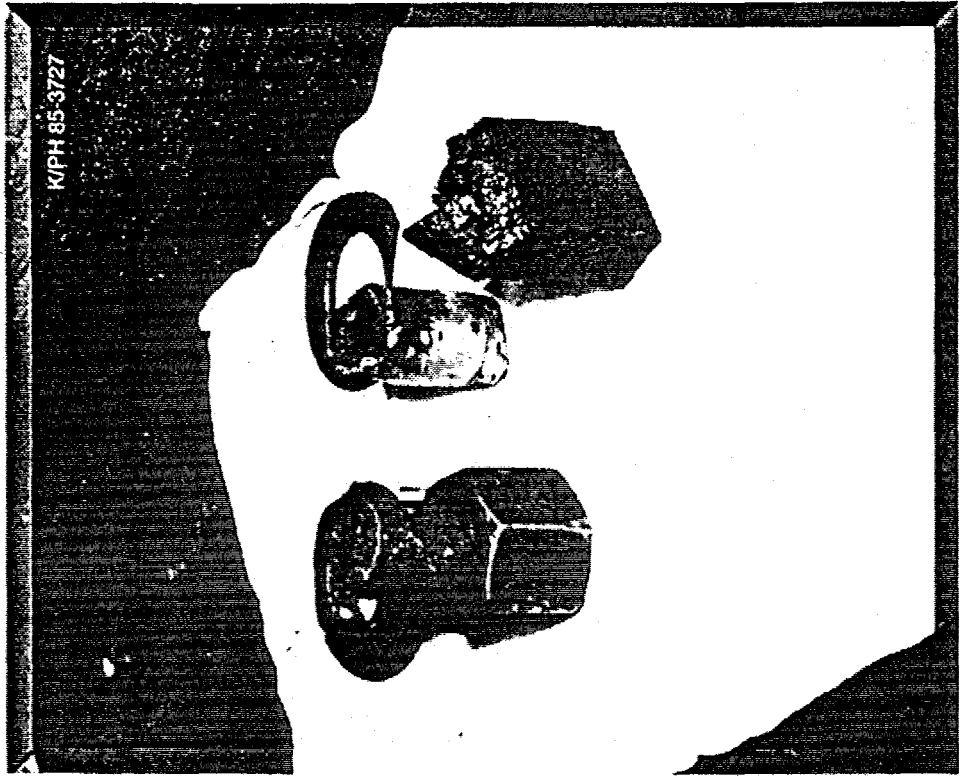
Fig. A.4. Shank of arbor fractured at bottom of cylinder.



oml



Latch Bolt Failure



Arbor Failure and Liner Fragment

Fig. A.5. DEMO IC component failures.



otm

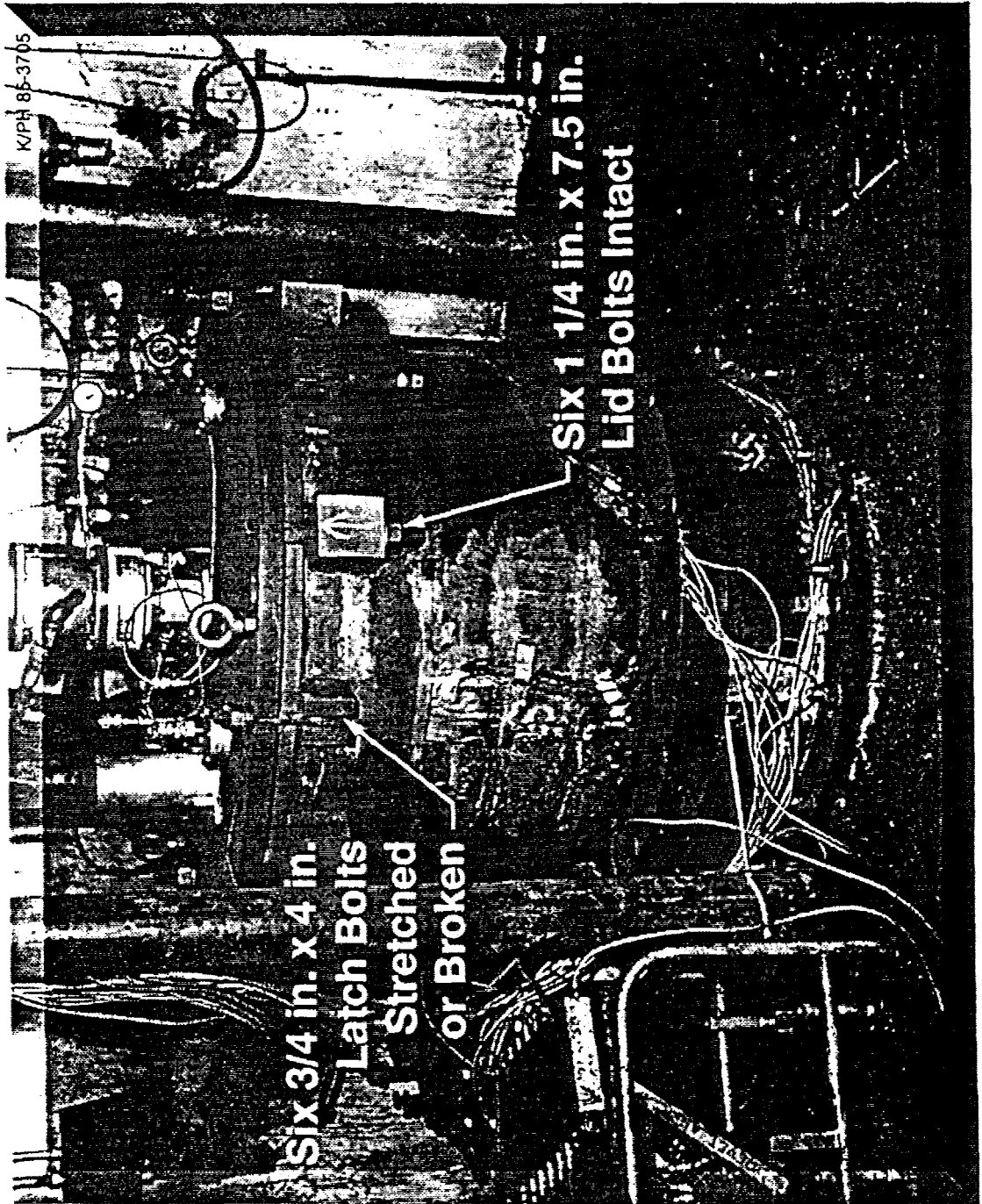


Fig. A.6. DEMO 1C after dust settled.



K/PH 85-3739



OTM

Fig. A.7. Dust and fragments embedded in revetment wall.



OTM

K/PH 85-3720

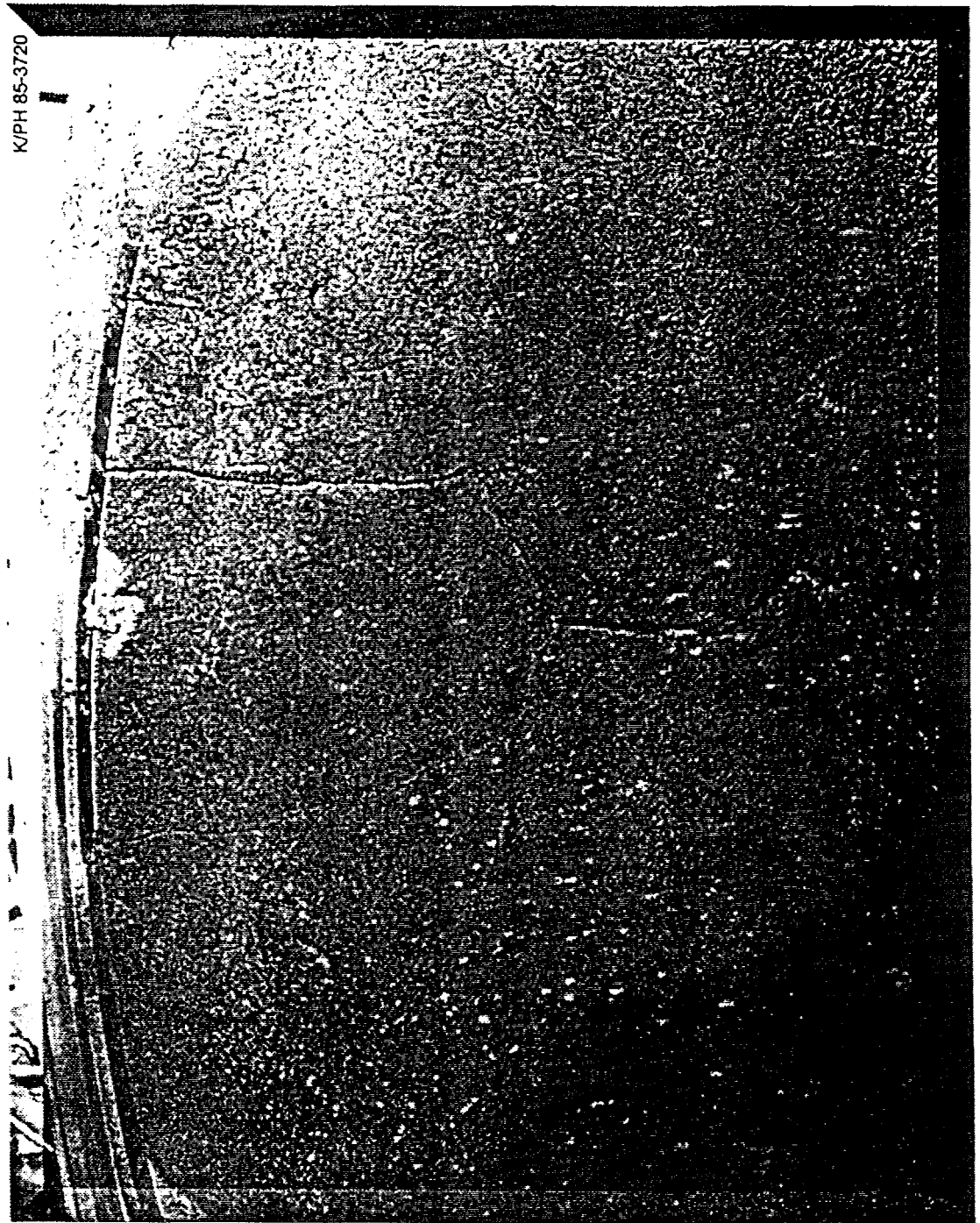


Fig. A.8. Shattered rotatable liner covered with flywheel burst products.



oml



Fig. A.9. Shattered rotatable liner after cleanup.

The locus of points formed by the intersection of the legs of all right triangles with a common hypotenuse form a semicircle with the hypotenuse as a diameter.

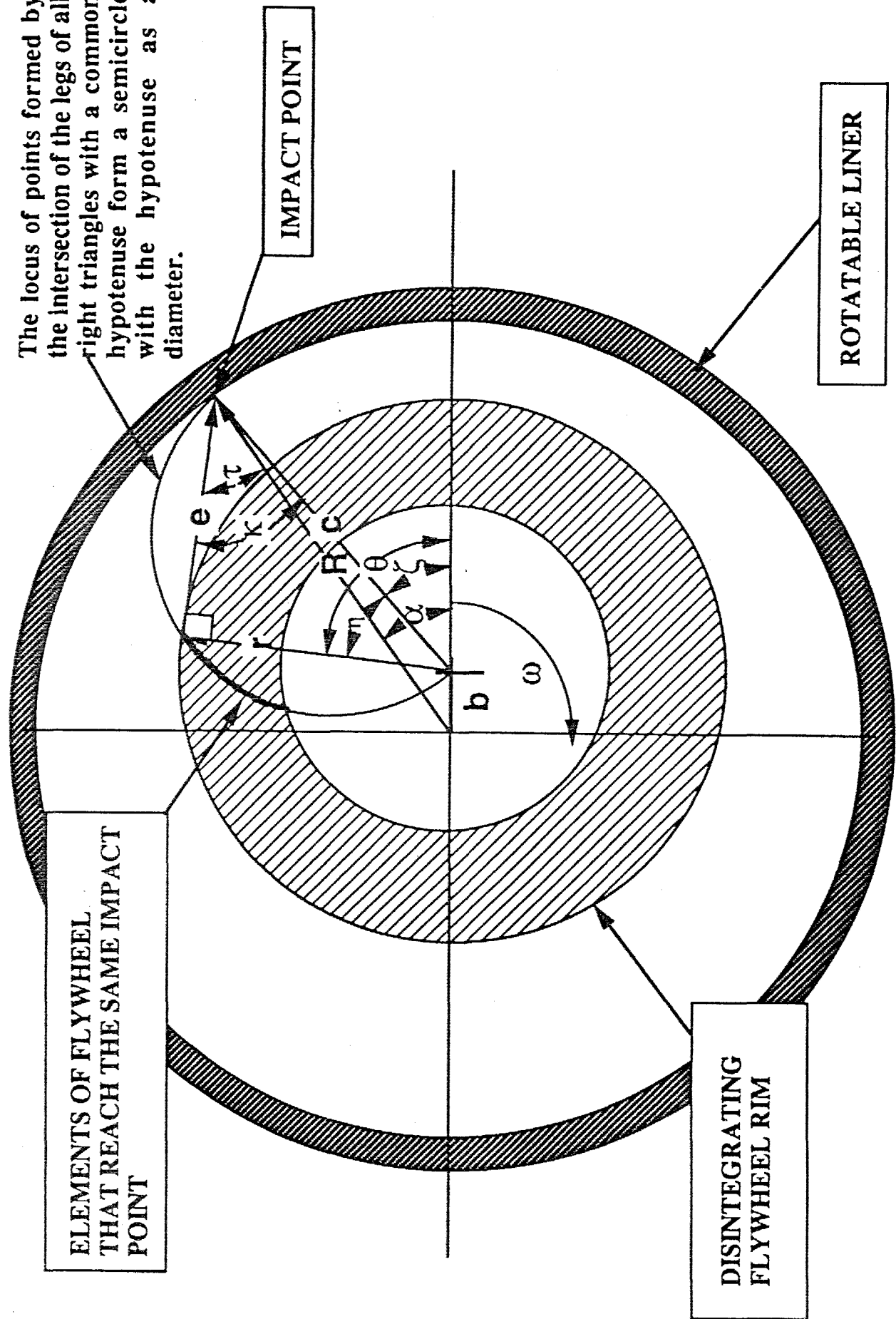


Fig. A.10. Disintegrating flywheel.

INTERNAL DISTRIBUTION

- | | |
|----------------------|----------------------------------|
| 1. M. A. Akerman | 11. D. U. O'Kain |
| 2. W. J. Allington | 12. J. W. McKeever |
| 3. J.B. Andriulli | 13. R. M. Schilling |
| 4. H. W. Blake | 14. J. T. Shaffer |
| 5. C. L. Coomer | 15. J. O. Stiegler |
| 6. R. G. Gilliland | 16. T. P. Sjoreen |
| 7. P. L. Goranson | 17. B. B. Thomas |
| 8. E. T. Grostick | 18-19. Laboratory Records |
| 9. M. D. Kass | 20. Laboratory Records Dept.--RC |
| 10. P. S. Litherland | 21. ORNL Patent Section |

EXTERNAL DISTRIBUTION

22. Robert Abboud, Common-Wealth Edison, 10 S. Dearborn, 35 FNE, Chicago, Illinois 60603
23. Ray Beach, NASA Lewis Research Center, MS 301-5, 2100 Brookpark Road, Cleveland, Ohio 44135
24. Marcel Belanger, Abacus Technology Services, 5454 Wisconsin Avenue, Suite 1100, Chevy Chase, Maryland 20879
25. Donald Bender, Trinity Flywheel Batteries, Inc., 10 Lombard Street, Suite 410, San Francisco, California 94111
26. Joe Beno, University of Texas, Center for ElectroMechanics, PRC/EME, Bldg. 133 (R7000) Austin, Texas 78712
27. Jack Bitterly, U.S. Flywheel Systems, Inc., 1125 Business Center Circle, Newbury Park, California 91320
28. John Coyner, American Flywheel Systems, Inc., 241 Koa Drive, Kodak, Tennessee 37764
29. Bob Davis, Honeywell, 8321 W. Foothill Drive, Peoria, Arizona 85382
30. Kent Decker, TRW Space & Defense, Bldg. R10, Rm 2045, 1 Space Park, Redondo Beach, California 90278
31. David Eisenhaure, SatCon Technology Corporation, 12 Emily Street, Cambridge, Massachusetts 02139
32. Ralph Flanagan, Flywheel Energy Systems, Inc., 190 Stafford Road, West, Unite 108, Ottawa, Ontario, Canada K2W 1AZ
33. Timothy Fox, California State University Northridge, 19111 Nordhoff Street, Mechanical Engineering Department, Northridge, California 91330
34. Roland Gravel, U.S. DOE Office of Transportation Technologies, DOE Flywheel Program Manager, EE32 (FORS), 1000 Independence Avenue, SW, Washington, D.C. 20585
35. William Grayer, Rosen Motors, 6430 Independence Avenue, Woodland Hills, California 91367

36. Ken Heitner, U.S. Department of Energy, EE-32, 5G-030, 1000 Independence Avenue, S.W., Washington, D.C. 20585
37. Jeff Hodgson, University of Tennessee, 414 Dougherty, Knoxville, Tennessee 37996-2210
38. John Hull, Argonne National Laboratory, Bldg. 335, 9700 S. Cass Avenue, Argonne, Illinois 60439
39. R. O. Hultgren, Deputy Assistant Manager, Energy Research & Development, Dept. of Energy, Oak Ridge National Laboratory, P.O. Box 2008, Oak Ridge, Tennessee 37831-6269
40. Adrian Hutchings, International Energy Systems Limited, Neston, South Wirral, England
41. Roy Kessinger, Visual Computing Systems, 9540 Hwy. 150, P.O. Box 250, Greenville, Indiana 47124
42. James Kirk, University of Maryland, Mechanical Engineering, College Park, Maryland 20742
43. Tom Kizer, Chrysler Corporation, 30900 Stephenson Highway, 463-00-00, Madison Heights, Michigan 48071
44. John Kramer, Argonne National Laboratory, 9700 S. Cass Avenue, Bldg. 207, Argonne, Illinois 60439
45. Terry Lorier, Rocketdyne Division, Rockwell International Corporation, 6633 Canoga Avenue, MC FA78, P.O. Box 7922, Canoga Park, California 91309-7922
46. Tom Martin, Boeing Defense & Space Group, P.O. Box 3999, M/S 82-32, Seattle, Washington 98124-2499
47. Office of Scientific and Technical Information, P.O. Box 62, Oak Ridge, Tennessee 37831
48. Joseph Olbermann, Unique Mobility, Inc., 425 Corporate Circle, Golden, Colorado 80210
49. Scott R. Penfield, Jr., P.O. Box 205, Signal Mtn, Tennessee 37377
50. John Price, University of Texas, Center for ElectroMechanics, PRC/EME, Bldg. 133, R7000, Austin, Texas 78712
51. Gerhard Reiner, Magnet-Motor GmbH, Petersbrunner Str. 2, 82349 Stanberg, Germany
52. Roman Rondiak, Albany International Research Company, 777 West Street, Mansfield, Massachusetts 02048-9114
53. Lewis Sibley, World Flywheel Consortium & Tribology Systems, Inc., 225A Plank Avenue, Paoli, Pennsylvania 19301-1726
54. J. Ray Smith, Lawrence Livermore National Laboratory, University of California, P.O. Box 808, L-641, Livermore, California 94551
55. Eric Sonnichsen, Test Devices, Inc., 6 Loring Street, Hudson, Massachusetts 01749
56. Mike Tamor, Ford Motor Company, SRL, MD 3435, Dearborn, Michigan 48121-2053
57. Tom Taylor, Bellcore, 445-South Street, IA-117G, Morristown, New Jersey 07960
58. Joseph Tecza, Mechanical Technical, Inc., 968 Albany-Shaker Road, Latham, New York 12110
59. Douglas Thorpe, Thortek, P.O. Box 20363, Knoxville, Tennessee 37940-1363
60. Andreas Vlahinos, NREL, Advanced Vehicle Systems, 1617 Cole Boulevard, 27/215, Golden, Colorado 80401-3393
61. Paul Wawrzonek, United Technologies Research Center, 411 Silver Lane, MS 129-22, East Hartford, Connecticut 06108
62. Jim Wolgemuth, General Motors Research and Development Center, Mail Code 480-106-A26, 30500 Mound Road, Warren, Michigan 48090-9055
63. Edward Zorzi, American Flywheel Systems, 5 Stonegate Road, Ballston Lake, New York 12019